Detachment of agglutinin-bonded red blood cells

III. Mechanical analysis for large contact areas

D. Berk* and E. Evans*‡

*Departments of Pathology and ‡Physics, University of British Columbia, Vancouver, British Columbia V6T 1W5, Canada

ABSTRACT An experimental method and analysis are introduced which provide direct quantitation of the strength of adhesive contact for large agglutinin-bonded regions between macroscopically smooth membrane capsules (e.g., red blood cells). The approach yields intrinsic properties for separation of adherent regions independent of mechanical deformation of the membrane capsules during detachment. Conceptually, the micromechanical method involves one rigid test-capsule surface (in the form of a perfect sphere) held fixed by a micropipette and a second deformable capsule maneuvered with another micropipette to force contact with the test capsule. Only the test capsule is bound with agglutinin so that the maximum number of cross-bridges can be formed without steric interference. Following formation of a large adhesion region by mechanical impingement, the deformable capsule is detached from the rigid capsule surface by progressive aspiration into the micropipette. For the particular case modeled here, the deformable capsule is assumed to be a red blood cell which is preswollen by slight osmotic hydration before the test. The caliber of the detachment pipette is chosen so that the capsule will form a smooth cylindrical "piston" inside the pipette as it is aspirated. Because of the high flexibility of the membrane, the capsule naturally seals against the tube wall by pressurization even though it does not adhere to the glass. This arrangement maintains perfect axial symmetry and prevents the membrane from folding or buckling. Hence, it is possible to rigorously analyze the mechanics of deformation of the cell body to obtain the crucial "transducer" relation between pipette suction force and the membrane tension applied directly at the perimeter of the adhesive contact. Further, the geometry of the cell throughout the detachment process is predicted which provides accurate specification of the contact angle θ_c between surfaces at the perimeter of the contact. A full analysis of red cell capsules during detachment has been carried out; however, it is shown that the shear rigidity of the red cell membrane can often be neglected so that the red cell can be treated as if it were an underfilled lipid bilayer vesicle. From the analysis, the mechanical leverage factor $(1 - \cos \theta_c)$ and the membrane tension at the contact perimeter are determined to provide a complete description of the local mechanics of membrane separation as functions of large-scale experimental variables (e.g., suction force, contact diameter, overall cell length). In a companion paper (Evans, E., D. Berk, A. Leung, and N. Mohandas. 1990. *Biophys. J.* 59:849–860), this approach was applied to the study of separation of large regions of adhesive contact formed between red blood cells by monoclonal antibodies and lectins.

INTRODUCTION

The process of cell–cell adhesion involves the assembly of membrane regions from positions of macroscopic separation (> 1 μm) to microscopic contact (gap dimensions less than a few nanometers). At microscopic contact, chemical bonding can occur through macromolecular cross-bridges to produce strong cell–cell attachment. Thus, even though cell surfaces may exhibit little initial attraction, agglutination after the surfaces are brought into intimate contact can be tenacious in opposition to separation forces. Phenomenologically, assembly and separation of large adhesive contact regions can be quantitated by the mechanical works to *form* and to *separate* a unit area of contact. However, these two work densities must be further refined to isolate the intrinsic properties of the adhesive contact. Here, two important factors must be recognized. First of all, a major portion of the mechanical work to assemble or separate cell contacts is the work necessary to deform the cell bodies to make the surfaces adjacent; the residual work is the energy associated with formation or separation of the microscopic surface–surface contact (1). Therefore, the effect of cell compliance must be analyzed to relate the forces applied to the cell body (and supported by the cell structure) directly to the forces that act at the periphery of the contact region. Displacement of these forces local to the contact region can then be used to define the intrinsic work for formation or separation of surface–surface contact (exclusive of the work of cell deformation). Secondly, formation or separation of contacts may not be accurately quantitated by changes in the apparent area of the contact region. Cell surfaces are often rough with numerous folds and wrinkles which compromise the definition of contact area. Therefore, to relate cell

Address correspondence and reprint requests to Dr. Evans.

0006-3495/91/04/861/12 $2.00

separation to the real change in contact area, the membrane surface should be macroscopically smooth.

If the mechanical compliance of the cell bodies can be specified and if the membrane surfaces are smooth, then measurements of forces involved in adhesion and separation of cell aggregates can be analyzed to give the intrinsic work densities for formation and separation of microscopic contact. In general, these two intensive properties of adhesion may not be equal. In the absence of external impingement forces, the work density to form membrane–membrane contact represents the cumulation of long-range microscopic attractions (e.g., van der Waals forces, macromolecular depletion forces, multivalent ion correlation forces, etc.) from macroscopic distances to final contact established by electrostatic and short-range steric repulsions (2, 2*a*, 3). This is a reversible free energy reduction w_a per unit area which is the natural "affinity" for formation of contact. On the other hand, the work per unit area to peel apart membrane surfaces may be greatly augmented by subsequent chemical bonding (agglutination) if separation proceeds at a rate faster than the equilibrium rate for dissociation of bonds (4, 4*a*, 5). (It is important to note that at complete equilibrium, chemical bonds only contribute a surface "spreading" pressure to the free energy reduction for contact formation [4, 4*a*, 5]. There is no contribution from chemical bonding energy because bonds are formed and dissolved at equal rates.) Viscous dissipation in the embedding solutions and cell surface structure can also greatly add to the mechanical energy requirements for separation. Thus, the work to separate a unit area of membrane contact becomes a phenomenological measure of the strength of adhesion referred to as a "fracture energy" w_f per unit area (6, 7, 7*a*). Based on thermodynamics, the fracture energy is always greater than or equal to the affinity for contact formation. For highly flexible membranes (where the bending stiffness is negligible), both properties of adhesion can be related to the membrane tension τ_m local to the contact region through the same mechanical leverage factor (given by the Young-Dupre equation),

$$(w_f \text{ or } w_a) = \tau_m (1 - \cos \theta_c), \quad (1)$$

where θ_c is the included angle between membrane surfaces. Thus, there will be two tension levels: one value is the tension *induced* by the affinity w_a as the contact spreads to an equilibrium area; the other value is the tension *required* to overcome the fracture energy w_f as the contact is separated (4, 4*a*). Likewise, there will be two different values for contact angle appropriate to spreading and separation of adhesive contact. Hence, measurement of tensions and contact angles, at equilibrium *and* as separation proceeds, are requisite parameters in the quantitation of adhesion.

Numerous physical techniques have been employed to study cell–cell adhesion. These have involved either external forces to detach adherent cells or analysis of equilibrium deformation of adherent cells (with well-known elastic properties) to deduce the stresses applied by the cell to the contact zone. In the first type of test, detachment forces were shear forces produced by flow of the adjacent liquids (8–10), acceleration forces by centrifugation (11–12), and suction forces by small micropipettes (13–15*a*). Although forces were measured directly, the unfortunate feature common to all of these experiments is that it was not possible to accurately determine the local stresses responsible for contact separation. Many aspects contribute to this deficiency: the cell geometry was not sufficiently symmetric to permit a tractable deformation analysis, the distribution of applied forces was unknown, the cell mechanical properties were not well defined or unduly complex, etc. By comparison, in the second type of test, equilibrium deformations of adherent cells were used as "transducers" for assay of adhesion energies (7, 7*a*, 13, 16, 17). These tests have only been reliable indicators of adhesion forces for red blood cells (or simple lipid bilayer vesicles) because most cells are not simple elastic bodies. The majority of cells are highly viscous with complicated rheological properties. The prominent exception is the mammalian red blood cell which has a reasonably well-defined membrane elasticity and a simple liquid interior (18). Hence, red cells can be used as convenient "transducers" for adhesion where the extent of deformation can be readily analyzed for symmetric geometries to yield the free energy required to create a unit area of contact (1, 7, 7*a*, 13, 16). However, this approach is restricted to the determination of the natural "affinity" between surfaces which is a lower bound for the "fracture" energy to separate contacts. Indeed, the approach must be used with caution because any slight mechanical impingement may force a cell to adhere well beyond the extent driven by weak natural attraction. This is clearly the case with antibody and lectin agglutinins: i.e., red cells appear not to spread spontaneously on one another beyond the extent to which they fit together without deformation. When forced together, the red cells are progressively agglutinated with a "tar-baby" effect driven by mechanical impingement (14, 19). Because of these deficiencies, we have developed an experimental method and analysis which will provide accurate measurements of both the affinity and the fracture energy properties for large contact regions. The essential ingredients are two macroscopically smooth, axisymmetric bodies. One of these is a flexible membrane capsule with a liquid interior (e.g., a red

blood cell or lipid bilayer vesicle); the other body can be any substance but with a rigid axisymmetric form. In the following sections, we introduce the experimental method and analysis; in a companion paper (19), we present results obtained with this approach for separation of large contact regions bonded by agglutinins specific to red cell surface receptors.

EXPERIMENTAL CONCEPT AND DESIGN

The concept and design of the separation experiment is demonstrated with red cells as shown in the videomicrographs, Fig. 1. The approach is to assemble the flaccid capsule with the rigid "test" body so that the geometry of the aggregate will remain axisymmetric throughout detachment. To ensure maximum cross-bridge formation without steric interference from blocked receptors, only the spherical test surface is bound with agglutinin molecules. In Fig. 1, the test surface is a swollen red blood cell that has been chemically fixed to create a rigid sphere. Chemical fixation restricts the motion of receptors and prevents receptor accumulation as the cells are separated. The agglutinin is bound only to these test particles from solution before the adhesion experiments. A micropipette is used to transfer one test particle to a microscope chamber free of agglutinin which contains the flaccid capsules. For red blood cells, the flaccid cells are slightly swollen by osmotic hydration to attain the appropriate surface area/volume ratio which will maintain the axisymmetric form shown in Fig. 1. A second pipette is then used to maneuver the agglutinin-free capsule to contact the test surface. This approach assures the juxtaposition of distinct "agglutinin" and "receptor" surfaces.

After adhesive contact, micropipette suction is used to separate the aggregate. The pipette suction pressure acts to increase membrane tension and to peel the flaccid-capsule membrane from the test surface. An innovative feature of this experimental arrangement is that the flaccid capsule fits snugly into the pipette to minimize fluid flow past the capsule without drag on the rim of the pipette at the entrance. Thus, the capsule acts as a "piston" within the pipette bore and naturally seals against the pipette wall without adherence because of internal pressurization. Negligible force is imparted by the glass wall of the pipette to the capsule membrane. Hence, friction and adhesion between the membrane and asperities at the pipette entrance are avoided and the entire suction force is applied to the capsule (given simply by the pipette suction pressure multiplied by the pipette cross-sectional area). Provided that the capsule surface maintains smooth contact with the pipette wall (without folds or creases), only a slow flow of liquid will occur between the capsule membrane and the pipette wall. Simple calculations (Appendix I) demonstrate that this flow will not significantly alter the applied force. To ensure patency of the seal against the pipette wall, the red cell is slightly preswollen to prevent buckling of the membrane. Consequently, the smooth symmetrical shape of the capsule can be predicted by rigorous analysis to obtain the distribution of membrane tension and surface orientation necessary for precise calculation of adhesion properties.

To evaluate the initial affinity between the surfaces, the flaccid cell is allowed to spread on the test surface without direct mechanical impingement. The initial tension induced in the capsule membrane provides a direct measure of the free energy reduction per unit area of contact formation (1, 16). To measure this tension and the subsequent fracture energy for separation of the contact, suction pressure is increased until a level is reached where the contact area begins to decrease. When bonded by specific agglutinins, mechanical impingement is necessary to produce large contact areas (cf. Fig. 1) and usually detachment will not occur at a fixed threshold level of suction force. The suction must be increased above the threshold; with each increase in suction, the membrane is progressively peeled from the test surface until the cell is completely detached (14, 19). At each stationary level of suction pressure, the cell shape does not change and the deformed state appears to be at mechanical equilibrium. For each step of the detachment, the suction pressure P_p, the diameter of the adhesive contact D_c ($=2r_c$), and the end-to-end length L of the flaccid cell are measured. As we will show, these measurements are sufficient to establish the membrane tension τ_m applied to the periphery of the contact region and the angle θ_c required to define the fracture energy density w_f. The fracture energy is obtained from the classical Young–Dupre equation provided the membrane is sufficiently flexible so that the elastic energy due to bending of the membrane near the contact can be neglected (1, 20). (Bending rigidity becomes negligible when the membrane tension satisfies the inequality $\tau_m > 8B/r_c^2$ where B is the elastic modulus for bending. For red blood cell membranes [$B \sim 10^{-12}$ dyn-cm], the elastic bending energy can be neglected when the work to separate the contact exceeds 10^{-3} ergs/cm^2 and the contact area exceeds 10^{-8} cm^2 [16, 20].) The sharp bend of the membrane at the periphery of the contact region (Fig. 1) indicates that the bending rigidity of the membrane can be neglected as the tension is increased. Finally, it is important to note that the fracture energy is a local measure of adhesive strength; consequently, it may vary over the course of detachment. Thus, a full analysis of cell deformation and compliance is required over the entire range of contact separation.

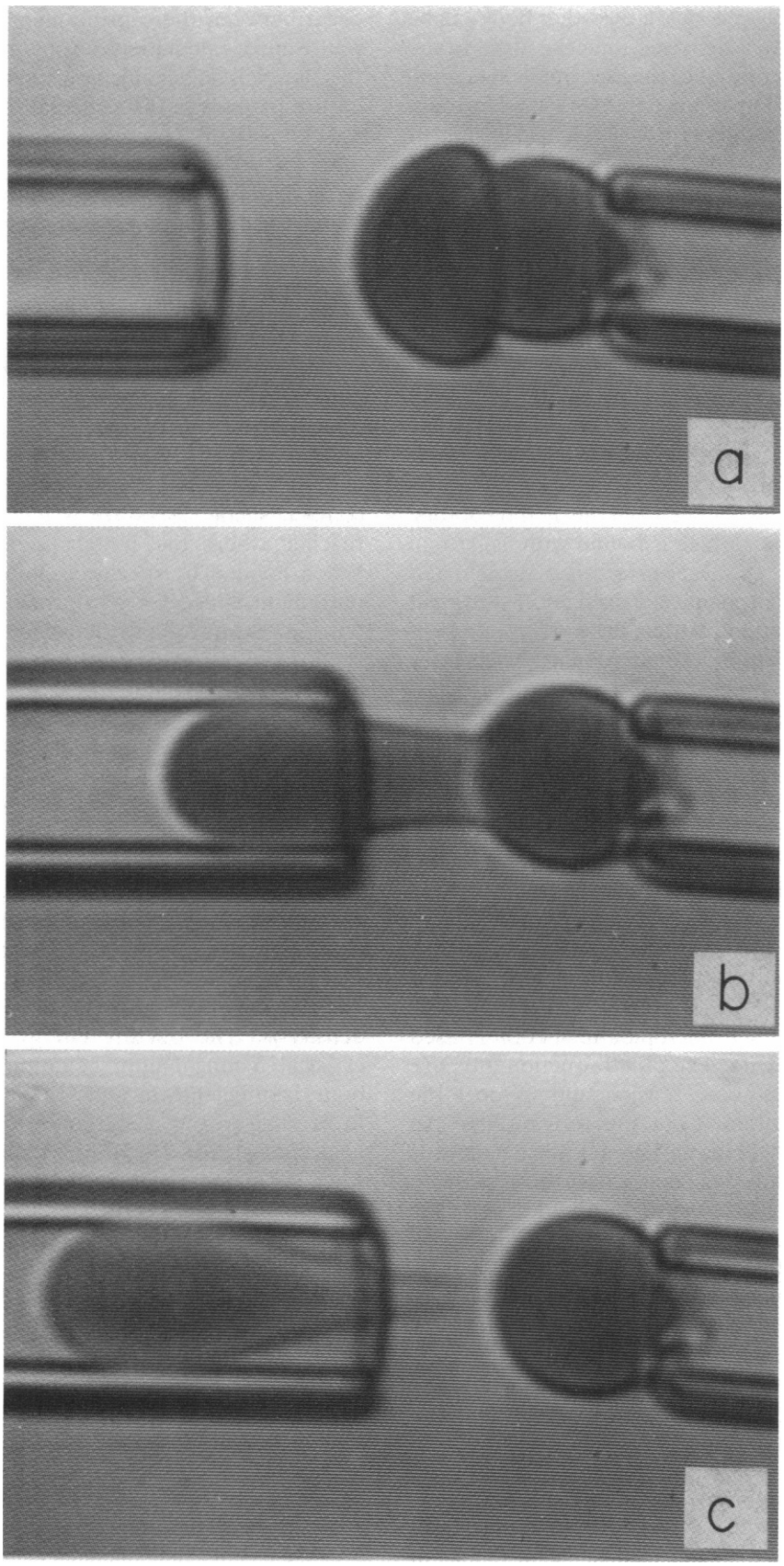
a
b
c

MECHANICAL EQUILIBRIUM AND CELL PRESSURIZATION

To analyze deformation of the flaccid membrane capsule, the first step is to introduce the equations of mechanical equilibrium (18) for the unsupported membrane section between the pipette and the adhesive contact (illustrated in Fig. 2). At a position on the axisymmetric surface (given by cylindrical coordinates—r,z), the first equation of equilibrium is the balance of forces normal to the membrane which relates the pressure P_c inside the capsule to the local membrane tensions multiplied by curvatures,

$$P_c = \tau_m \cdot c_m + \tau_\phi \cdot c_\phi. \tag{2}$$

τ_m, τ_ϕ are the principal tensions which act tangent to the meridional contour and latitude circle, respectively. The corresponding principal curvatures (c_m, c_ϕ) are defined by,

$$c_m = \frac{\partial \theta}{\partial s}$$
$$c_\phi = \frac{\sin \theta}{r} \tag{3}$$

in terms of the intrinsic curvilinear coordinates (s, θ) shown in Fig. 2. The curvilinear coordinates are related to the spatial coordinates by the following differentials:

$$dr = \cos \theta \cdot ds$$
$$dz = \sin \theta \cdot ds.$$

The other equation of equilibrium comes from the balance of forces tangent to the meridional contour,

$$\frac{\partial (r\tau_m)}{\partial s} - \tau_\phi \cdot \frac{\partial r}{\partial s} = 0 \tag{4}$$

or equivalently,

$$\frac{\partial (r\tau_m)}{\partial r} = \tau_\phi.$$

The equations of mechanical equilibrium can be rearranged to give relations for the membrane tensions in terms of membrane geometry, i.e.,

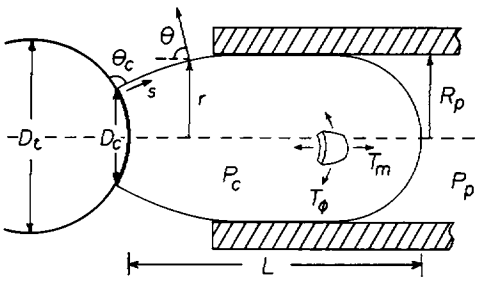

FIGURE 2 Geometry of the adherent capsule. The membrane capsule is axially symmetric and characterized by these experimental parameters: the test particle diameter D_t, the adhesive contact diameter D_c, the pipette diameter $2R_p$, and the end-to-end length L of the capsule. Local positions on the membrane are specified by the curvilinear distance s along a meridian and the radial distance r from the pipette axis. The membrane orientation is represented by the angle θ formed between the surface normal vector and the symmetry axis. The state of membrane tension at any location is given by meridional and circumferential components (τ_m and τ_ϕ).

$$\tau_m = (P_c \cdot r^2 + f/\pi)/(2r \cdot \sin \theta)$$
$$\tau_\phi = \frac{d}{dr}[(P_c \cdot r^2 + f/\pi)/(2 \cdot \sin \theta)], \tag{5}$$

where P_c is the uniform pressure inside the capsule (relative to the outside-ambient pressure) and f is the total axial force which is required to hold the test surface at a fixed position. The total axial force is the pipette suction force $f = \pi R_p^2 P_p$. (The drag force produced by the slow flow of liquid through the thin annulus between the capsule membrane and pipette wall causes a slight reduction of membrane tension along the cylindrical section.) It is useful to scale these equations to dimensionless forms as follows:

$$\tilde{\tau}_m \equiv 2\tau_m/P_p \cdot R_p, \quad \tilde{\tau}_\phi \equiv 2\tau_\phi/P_p \cdot R_p$$
$$\tilde{P}_c \equiv P_c/P_p, \quad \tilde{r} \equiv r/R_p.$$

Hence,

$$\tilde{\tau}_m = (\tilde{P}_c \cdot \tilde{r} + 1/\tilde{r}) / \sin \theta$$
$$\tilde{\tau}_\phi = \frac{d}{d\tilde{r}}[(\tilde{P}_c \cdot \tilde{r}^2 + 1) / \sin \theta]. \tag{6}$$

FIGURE 1 Videomicrographs of capsule adhesion to, and separation from, a rigid test surface. The test surface (held by the pipette on the right) was a red blood cell chemically fixed in the form of a rigid sphere and then bound with agglutinin molecules. The flaccid capsule (maneuvered with the pipette on the left) was a normal red blood cell osmotically preswollen by about 20% (i.e., volume ~ 115 μm³). (*a*) The deformable capsule was forced by positive pipette pressure against the rigid test surface to produce a large area of adhesive contact. (*b*) Next, the capsule was aspirated into the pipette (~4.6 μm diam) with sufficient suction to reduce the contact area. (*c*) The suction pressure was further increased to a maximum value beyond which detachment occurred. (The capsule shapes in *b* and *c* appeared to be at mechanical equilibrium with no obvious motion.)

It is clear from the equation for meridional tension that pressurization ($P_c > 0$) of the capsule creates a greater separation tension local to the adhesive contact than that implied by the pipette suction alone. As Eqs. 6 show, the variation of membrane tension over the contour is determined by the instantaneous (deformed) geometry of the capsule. The next step in the analysis is to relate the tensions to the *change* in capsule geometry through elastic constitutive equations.

MEMBRANE CONSTITUTIVE BEHAVIOR

Cell and synthetic bilayer membranes exhibit the common feature that the surface area can only be expanded to a small extent ($\leq 3\%$) by large tensions above which rupture occurs (18). Thus, for practical calculations, the membrane can be treated as an incompressible surface where local areas are unchanged by deformation (i.e., extension of surface elements in-plane must be accompanied by commensurate narrowing of the elements). As an incompressible surface, the isotropic (mean) tension $\bar{\tau}=(\tau_m + \tau_\phi)/2$ becomes arbitrary and is replaced by the geometric constraint for fixed differential areas, i.e.,

$$2\pi r \cdot ds = 2\pi r_0 \cdot ds_0, \tag{7}$$

where (r, s, and r_0, s_0) are the surface coordinates of common material points defined for the instantaneous and initial (reference) contours, respectively. The consequence is that the extension of the membrane along the meridian (given by $\lambda_m = ds/ds_0$) is precisely related to the local ratio of circumferences between the deformed and undeformed geometries ($\lambda_\phi = 2\pi r_0$), i.e.,

$$\lambda_m = \lambda_\phi^{-1} = r_0/r. \tag{8}$$

Therefore, Eqs. 7 and 8 describe the deformation field for the membrane in terms of *changes* in geometry relative to the undeformed shape. For example, the change in membrane orientation is given by

$$\cos\theta = \frac{\cos\theta_0}{\lambda_m^2} - \frac{r_0}{\lambda_m^3} \cdot \frac{d\lambda_m}{ds_0}, \tag{9}$$

where (θ, θ_0) are angles defined for the deformed and undeformed contours, respectively.

Because the surface is incompressible, local elements of the membrane deform by in-plane shear and bending (18). The measure of shear deformation is given explicitly by the finite shear strain $\epsilon_s = (\lambda_m^2 - \lambda_m^{-2})/4$. The response of the membrane in shear is represented by the relation between the deviatoric tension $\tau_s = (\tau_m - \tau_\phi)/2$, or shear force resultant, and the shear deformation. The first order elastic relation is characterized by an elastic shear modulus μ for the membrane, i.e.,

$$\tau_s = 2\mu \cdot \epsilon_s = (\tau_m - \tau_\phi)/2. \tag{10}$$

For surface liquids (lipid bilayers with fluid acyl chains), the shear modulus is identically zero. For red blood cell membranes, the modulus has been measured to be on the order of 6×10^{-3} dyn/cm (21). Therefore, deformation of the unsupported membrane capsule is specified by Eqs. 7–9 and the appropriate combination of Eqs. 6,

$$\tilde{\mu}\left[\left(\frac{\tilde{r}}{\tilde{r}_0}\right)^2 - \left(\frac{\tilde{r}_0}{\tilde{r}}\right)^2\right] = \tilde{r} \cdot \frac{d}{d\tilde{r}}\left[(\tilde{P}_c \cdot \tilde{r} + 1/\tilde{r}) / \sin\theta\right]. \tag{11}$$

As is apparent from the dimensionless equations for membrane tensions, the effect of membrane shear rigidity is scaled by the ratio $\tilde{\mu} = \mu/P_c R_p$. Thus, when the product of pipette suction x pipette radius is much greater than the shear modulus, the membrane deforms as if it were an incompressible fluid surface (like lipid bilayers). In the limit ($\tilde{\mu} \to 0$) of complete pressurization, Eq. 11 reduces to

$$\sin\theta = \frac{(\tilde{P}_c \cdot \tilde{r}^2 + 1)}{\tilde{r} \cdot (\tilde{P}_c + 1)} \tag{12}$$

which describes a surface of constant mean curvature ($c_m + c_\phi$ = constant). Eqs. 11 and 12, accompanied by the restriction on local surface dilation imply universal families of membrane shapes which only depend on the internal pressure of the capsule.The specific value for internal pressure is dictated by the auxiliary requirement that the capsule volume is constant (because pressures are not sufficient to force significant amounts of water out of the capsule against osmotic activity and permeability restrictions). Since the total capsule area and volume remain constant throughout detachment, there will be a unique relation between cell end-to-end length L and the diameter of the adhesive contact D_c. Likewise, membrane orientation θ and the contact angle θ_c local to the adhesive site will be unique functions of the capsule extension. Consequently, analytical prediction of capsule geometry throughout detachment provides accurate specifications for angles and tensions local to the contact zone *plus* a self-consistent check on the values estimated for capsule area and volume.

CAPSULE GEOMETRY

Below the limit of full pressurization of the capsule, both the isotropic and deviatoric (shear) tensions are required to balance forces in the membrane. Eqs. 7 and 11

provide a set of relations that yield capsule shape, internal pressure, and tension distribution. Solutions to these equations depend on the contact diameter, the pipette radius, pipette suction pressure, capsule area, and volume. An iterative procedure is used to determine capsule geometry. To do this, the flaccid capsule is divided into four distinct regions (Fig. 3): the membrane region that forms the contact zone, the unsupported section between the test surface and the micropipette, the cylindrical section adjacent to the micropipette wall, and a hemispheroidal cap inside the pipette. Three of these sections are simple geometric forms for which the surface areas and volumes can be easily calculated. Only the shape of the unsupported section must be obtained by numerical quadrature. When the capsule is sufficiently pressurized, the shape of the unsupported region is calculated by direct integration of the equation for a surface with a constant mean curvature, Eq. 12. At lower tension levels, a finite-difference algorithm is used to compute the geometry of the unsupported region because of the complexity introduced into the equations by the elastic shear rigidity (see Appendix II). Finally, the iterative procedure is to vary the dimensionless internal pressure $\tilde{P}_c$ (for fixed values of contact diameter D_c and capsule area) until the appropriate value is obtained for the capsule volume.

RESULTS AND DISCUSSION

With the numerical procedure outlined above, the complete shape of the flaccid capsule is calculated given the diameter of the adhesive contact, pipette diameter, and the capsule surface area and volume. Fig. 4 presents a sequence of shapes computed for the situation similar to that in Fig. 1. Given the shape, the distribution of meridional tension is calculated along the free contour to provide the value of tension at the perimeter of the adhesive contact as well as the contact angle included between the surfaces. In the analysis of experiments, the crucial unknown variables are the cell surface area and volume. Often, these cannot be accurately measured by direct observation of small-size capsules (like red cells) because of optical diffraction limitations. However, the initial estimates for area and volume can be refined by correlation of predicted vis a vis observed relations between the end-to-end extension of the capsule and the contact diameter over the course of detachment. The total capsule length can be measured with reasonable accuracy and compared with the length predicted by computation of cell shape as a function of contact diameter for various values of surface area and volume. Ideally, only two sets of values for capsule length and contact diameter are needed to specify the area and volume of the capsule. Hence, the correlation of capsule length vs. contact diameter over the full range of detachment provides a restrictive test of these parameter values. The geometric relation between cell extension and contact diamter is shown in Fig. 5 for a red cell aspirated into a specific-size pipette as a function of cell volume.

A practical consideration in experiment analysis is that computation of capsule geometries in the low tension range (where shear rigidity is important) can be

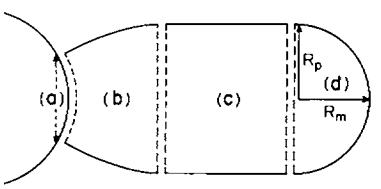

FIGURE 3 Segmentation of the cell shape used in the computational algorithm. The adherent portion of the capsule (*a*) and the cylindrical portion inside the pipette (*c*) follow contours of rigid surfaces. The cap (*d*) within the pipette is approximated as an oblate spheroid with eccentricity that depends on membrane shear rigidity vis a vis internal pressure. The portion (*b*) is chosen to satisfy the equations of mechanical equilibrium for an "unsupported" membrane.

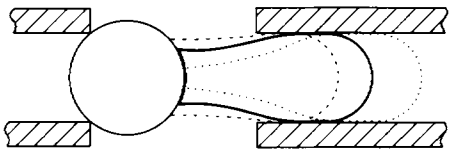

FIGURE 4 Capsule geometry predicted in the course of detachment for parameters comparable to the experiment illustrated in Fig. 1.

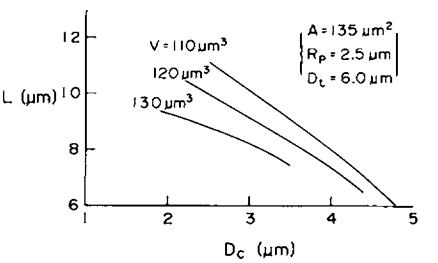

FIGURE 5 Functional relation predicted for end-to-end length of the deformable capsule vs. contact diameter where the capsule area was held constant at $A = 135\ \mu m^2$ and the internal diameter of the pipette was 5.0 μm. Separate curves are shown for three capsule volumes that represent increases over the normal red cell volume in isotonic media (i.e., ~94 μm^3). Swelling of the cell results in lower extensions into the pipette.

expensive and time consuming. By comparison, computations are relatively simple and direct for fully pressurized capsules. Thus, it was important to determine the conditions under which a capsule can be considered fully pressurized and shear rigidity neglected. To establish the requisite conditions, we examined the relation between dimensionless tension at the contact perimeter and the dimensionless shear modulus for a wide range of capsule sizes and contact diameters. The finite-difference solutions showed that when $\tilde{P} \equiv 1/\tilde{\mu} > 1$, the capsule rapidly approaches the fully pressurized approximation where the shape and tension are almost identical to those calculated for a surface with no shear rigidity. Fig. 6 shows the cross-over range of suction pressure where membrane shear rigidity becomes less important. In this figure, the dimensionless tension at the perimeter of the adhesive contact is plotted vs. the reciprocal of the dimensionless shear rigidity (i.e., the dimensionless suction pressure). Fig. 6 *a* gives values expected for a relatively "unswollen" cell. Fig. 6 *b* is a plot of results for a more "swollen" cell. The geometries modeled for Fig. 6 represent the useful range of red cell

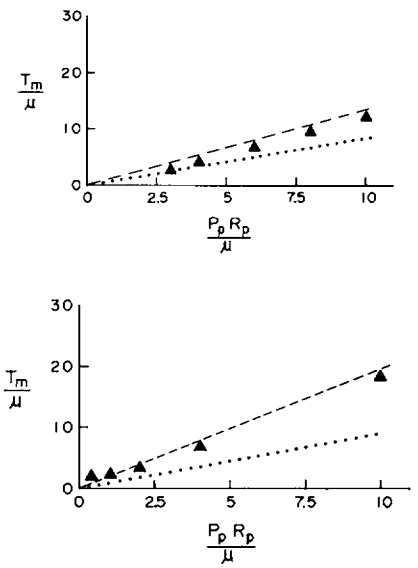

FIGURE 6 The dimensionless tension applied at the contact perimeter is plotted vs. the dimensionless pipette suction pressure. The results represent different solutions: a pressurized capsule with *no* membrane shear rigidity (*dashed curve*); a capsule with zero internal pressure where the volume was allowed to change (*dotted curve*); and the complete finite-difference solution *with* membrane shear rigidity and fixed internal volume (*closed triangles*). (*a*) The capsule geometry was chosen to represent a slightly swollen red cell (area = 135 μm^2, volume = 115 μm^3). (*b*) The capsule geometry was chosen to represent a more swollen red cell (area = 135 μm^2; volume = 130 μm^3). (The internal diameter of the pipette was 5.0 μm and the contact diameter was fixed at 3.0 μm in both cases.)

volumes for a typical pipette size which would be employed in experiments.

In Fig. 6, three solutions are plotted: the results for a "pressure-less" cell (where the cell volume was allowed to change); results for the fully pressurized capsule with no membrane shear rigidity; results for the "complete" solution with shear elasticity and fixed internal volume. Obviously, the "pressure-less" and "pressurized" solutions form lower and upper bounds to the exact solution. For the less swollen capsule (Fig. 6 *a*), the complete solution yields internal pressure values that are initially negative when the dimensionless suction pressure is below $\tilde{P} = 2$. For actual deformations, negative internal pressures would cause membrane buckling and folding (although membrane bending stiffness could stabilize the axisymmetric shape for very small negative pressures); thus, axisymmetric shapes calculated where internal pressures are negative must be regarded as "unphysical." For the situation represented in Fig. 6 *a*, the cell develops positive internal pressures when the dimensionless suction pressure exceeds $\tilde{P} = 2$. Further for $\tilde{P} > 3$, the tension closely approximates the solution predicted for the fully pressurized capsule. Dimensionless tensions for the two solutions always differ by an amount on the order of unity but the fractional difference becomes negligible for $\tilde{P} > 3$. In contrast to Fig. 6 *a*, the more swollen red cell represented by the curves in Fig. 6 *b* always possesses positive internal pressure even before the suction force is applied. As before, the dimensionless tension values vs. dimensionless suction pressure closely follow the fully pressurized solution for $\tilde{P} > 2$. Flaccid red cells with less volume than used for Fig. 6 *a* would easily fold at low suction pressures and be visibly separated from the pipette walls at higher suctions. On the other hand, red cells more swollen than that used for Fig. 6 *b* would not be able to completely enter the pipette without area dilation. Hence, red cell volumes for these two cases represent the useful range of cell size. The principal effect of shear rigidity is to reduce the contact angle by a few degrees when the tensions are low. Above dimensionless suction pressure $\tilde{P} = 4$, the contact angle (between the adherent capsule and test surface) usually deviates by $< 2°$ from the result for the fully pressurized capsule. Fig. 7 illustrates the relation between contact angle and end-to-end length for a typical red cell volume and pipette size. (Note, shear rigidity remains significant in the narrow neck region of the deformed cell when the contact area is small, $D_c < 2$ μm [c.f. Fig. 1 *c*]; this is indicated by the dashed portion of the curve in Fig. 7. A useful pressurized-cell approximation is to require the minimum diameter of the neck to be a cylinder with cross-section equal to the contact area.)

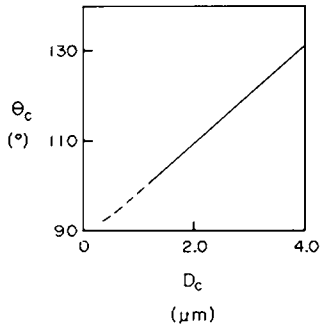

FIGURE 7 Functional relation predicted for the included angle θ_c between membrane surfaces at the perimeter of the contact vs. diameter D_c of the adhesive contact where the capsule area was held constant at $A = 135\ \mu m^2$ and the internal diameter of the pipette was 4.6 μm. The cell volume was held fixed at $115/\mu m^3$. These parameters were chosen to model the situation shown in Fig. 1. The dashed portion of the curve shows the region where shear rigidity affects the geometry.

CONCLUSIONS

The results from the numerical computations show that for dimensionless suction pressures greater than $\tilde{P} =$ 3–4, the capsule is essentially fully pressurized and the shape is almost identical to that of a simple fluid membrane vesicle with the same area and volume. For dimensionless suction pressures greater than $\tilde{P} = 3$, the relation between the contact diameter at the adhesion site and the end-to-end length of the cell is an easily specified function of red cell surface area and volume. As such, experimental measurement of cell length vs. contact diameter can be used to refine initial estimates of the surface area and volume which are required in the analysis of capsule deformation. Further, the prediction of capsule geometry provides an accurate relation for contact angle as a function of either end-to-end length or contact diameter which circumvents the uncertain measurement of membrane orientation near the adhesive contact. Because of the design of this experiment, contact angles remain slightly greater than 90° throughout the detachment. Thus, the mechanical work to separate a unit area of contact will be approximately given by the value of membrane tension local to the contact zone. The optimum design for red cell separation experiments includes a pipette diameter of ~4.5–5.0 μm and cell volumes preswollen by 20–30% (so that the cell will form a smooth contour adjacent to the walls of the pipette). Under these conditions, mechanical impingement of the cell can produce initial contact diameters of as much as 4–5 μm.

Complete calculations show that the membrane tension local to the contact perimeter is well approximated by the value for the isotropic tension found for the fully pressurized capsule minus a constant equal to the membrane elastic shear modulus (for $\tilde{P} > 2$). For red cells agglutinated by antibodies or lectins, recent separation tests (19) show that suction pressures must be increased significantly above 100 dyn /cm² to separate the cells which corresponds to $\tilde{P} > 4$. Thus, the simplified calculation for a fully pressurized capsule is appropriate for these situations. However, the experimental approach is not well-suited for red cell separation tests when lower values of suction are used (tensions <0.01 dyn /cm). For low tensions, the membrane shear rigidity is significant and analysis of membrane deformation requires the complete finite-difference approach. Also at low tensions, membrane bending rigidity becomes important and will lead to large radius bends at the perimeter of the contact zone. (For the red cell, bending stiffness becomes a major factor when the tension level is reduced to the order of 10^{-3} dyn /cm. Even for tension levels up to 0.01 dyn /cm, the bending stiffness may affect the curvature local to the contact perimeter.) Another practical concern is that below dimensionless suction pressures of $\tilde{P} =$ 2–4, the cell membrane may buckle to prevent a smooth seal against the pipette wall.

APPENDIX I

Effect of fluid leakage around the pressurized capsule

In the experiment, the capsule fills the mouth of the pipette like a piston so that a portion of the cell assumes a cylindrical shape; but, there will be a small gap between the membrane and the pipette wall. Even though the membrane appears to contact the pipette walls, water will slowly flow into the pipette through this thin gap. (Observation of small suspended particles inside the pipette near the capsule shows that there is no detectable convection or drift, only Brownian motion. This demonstrates that the flow of water past the capsule is *very* small.) The effects of the flow are (*a*) to reduce the total pressure force that acts across the capsule and (*b*) to create a fluid drag on the surface of the capsule which produces a gradient in membrane tension. Because the gap between the membrane and the glass is below optical resolution in the microscope, the size of the gap and effects of the fluid leak can only be estimated.

The pipette suction pressure is the difference between the pressure in the microscope chamber and the pressure in a reservoir distant from the pipette. If there is no flow into the pipette, the total pressure difference is across the capsule in the pipette tip. However, with a small flow rate Q into the pipette, there will be a continuous pressure drop along the entire pipette and tubing that leads to the reservoir. The pressure drops in the cylindrical sections can be estimated from the Poiseuille equation for flow, i.e.,

$$\Delta P = 8\eta \cdot Q \cdot L/\pi R^4, \qquad \text{(A1)}$$

where η is the fluid viscosity, L is the length, and R is the radius of a particular section. For flow in the thin annular gap of width h, the

pressure drop is approximated by

$$\Delta P_A = 6\eta \cdot Q \cdot L/\pi R \cdot h^3. \quad \text{(A2)}$$

In addition, there will be a pressure drop from the microscope chamber to the gap entrance at the pipette tip, approximated by

$$\Delta P_E \sim \eta \cdot Q/2\pi R \cdot h^2 \quad \text{(A3)}$$

which is derived from the exact solution for convergent flow between perpendicular walls to a "sink" at the corner (22). Analysis of the total system pressure drop follows the schematic illustrated in Fig. A1. It includes the pressure drops for the entrance region exterior to the gap at the pipette tip ΔP_E, the annular gap around the capsule inside the pipette ΔP_A, a narrow channel of the pipette downstream of the capsule ΔP_N, and a large caliber cylinder that leads to the pressure reservoir ΔP_W. For conservative estimate, the radii of the annulus and the narrow channel are both taken as $R_N \simeq R_p \sim 2.5$ μm; the length L_A of the annular gap is on the order of 1–2 μm; the length of the narrow channel region is ~10–20 μm. The size of the large caliber section is at least $R_w > 200$ μm with a length $L_w < 1$–10 cm. Finally, the thickness h of the gap must be on the order of 0.1 μm or less because it is smaller than the optical diffraction limit. Based on these values, ratios of pressure drops in the various regions to that through the annular gap are calculated as follows:

$$\Delta P_W/\Delta P_A \sim (L_W R_p h^3)/(L_A R_W^4) \sim 10^{-6}$$
$$\Delta P_N/\Delta P_A \sim (L_N h^3)/(L_A R_p^3) \sim 10^{-3}$$
$$\Delta P_E/\Delta P_A \sim h/12L \sim 10^{-2}.$$

Clearly, nearly all of the suction pressure acts across the annular gap region and the entrance-flow pressure drop can be neglected if the cylindrical length of the gap is much greater than the gap thickness. Likewise, corrections to the total force supported by the adhesive contact can be shown to be on the order of $-h/2L_A$ and $-h/R_p$. The first small reduction in force is the pressure drop correction for the entrance flow (adjusted by a factor of one-half for the local drag on the capsule surface); the second reduction in force is the correction for capsule cross-section (again offset by a factor of one-half because of the fluid drag on the capsule along the gap).

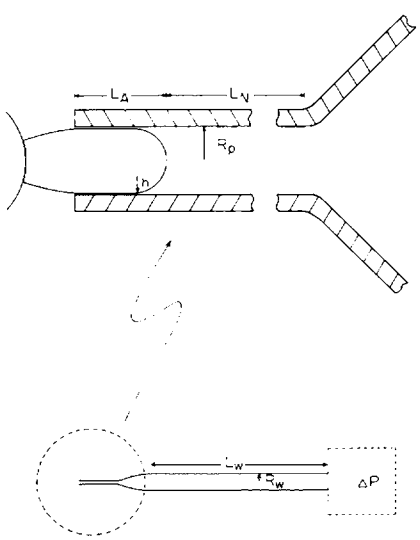

FIGURE A1 Schematic of the pipette system used for analysis of pressure distribution. Appropriate dimensions are given in the text.

APPENDIX II

Finite-difference approach to obtain membrane shape

Most of the shape of the capsule is imposed by rigid surfaces, e.g., adhesion to the test surface and pressurization against the pipette walls. The shape of the unsupported membrane from the perimeter of the adhesive contact to the pipette is variable and must be chosen to satisfy the equations of mechanical equilibrium at each point on the surface. Calculation of the shape is accomplished by means of a finite-difference algorithm for the complete equations with membrane shear rigidity. The unsupported region of the capsule is approximated as a series of conical sections, each with a mean radius r and surface orientation angle θ at a meridional position s (Fig. 2). The surface area and volume of this region of the cell are simply the sums of the areas and volumes for each of the conical sections. These sections are mapped back to the undeformed cell shape to determine the reference coordinates s_0 and r_0, the initial meridional position and the initial radial distances from the axis of symmetry. This "map" establishes the local extension (shear deformation) of each membrane section which specifies the shear resultant τ_s as given by Eqs. 8 and 10. To preserve symmetry, the undeformed reference shape is taken as either a sphere or a biconcave disk oriented with its axis of symmetry aligned with the micropipette axis.

The balance of forces along the axis of symmetry can be combined with the local mechanical equilibrium for forces normal to the membrane to obtain a single equation for the shear force resultant,

$$\epsilon = 4\tilde{\tau}_s \cdot \sin^2\theta - (\tilde{r}^2\tilde{P}_c + 1)\frac{\partial\theta}{\partial\tilde{s}} + (\tilde{r}^2\tilde{P}_c - 1)\frac{\sin\theta}{\tilde{r}}, \quad \text{(B1)}$$

where distances are scaled by R_p, pressures by P_p, and tensions by $P_p R_p/2$. The residual function is used to obtain the solution for the membrane shape and the tensions at any point. The equilibrium shape is found by specifying an initial shape for the cell (e.g., the shape of a *fully* pressurized cell). Then, the shape (given by the coordinates r, θ) is allowed to relax to the equilibrium solution that gives $\epsilon = 0$ at each point. Computationally, this is accomplished by introducing surface dissipation (viscous damping) into the shear force resultant.

For small changes in r and θ, the perturbation in the function ϵ is given by its first order linear expansion:

$$\Delta\epsilon = \frac{\partial\epsilon}{\partial\tilde{r}}\cdot\Delta\tilde{r} + \frac{\partial\epsilon}{\partial\theta}\cdot\Delta\theta + \frac{\partial\epsilon}{\partial\left\{\frac{d\theta}{d\tilde{s}_0}\right\}}\cdot\Delta\left\{\frac{d\theta}{d\tilde{s}_0}\right\} + \frac{\partial\epsilon}{\partial\tilde{P}_c}\cdot\Delta\tilde{P}_c$$

$$\frac{\partial\epsilon}{\partial\tilde{r}} = \frac{1}{\tilde{r}}\left\{\left\{(\tilde{r}^2\tilde{P}_c + 1)\frac{\sin\theta}{\tilde{r}} - (3\tilde{r}^2\tilde{P}_c + 1)\frac{\partial\theta}{\partial\tilde{s}} - 4\sin^2\theta\cdot\left\{\lambda_m\frac{\partial\tilde{\tau}_s}{\partial\lambda_m}\right\}\right\}\right.$$

$$\frac{\partial\epsilon}{\partial\theta} = 8\tilde{\tau}_s\cdot\sin\theta\cdot\cos\theta + (\tilde{r}^2\tilde{P}_c - 1)\frac{\cos\theta}{\tilde{r}}$$

$$\frac{\partial \epsilon}{\partial \left(\frac{d\theta}{d\tilde{s}_0}\right)} = -\frac{(\tilde{r}^2\tilde{P}_c + 1)}{\lambda_m}$$

$$\frac{\partial \epsilon}{\partial \tilde{P}_c} = \tilde{r}^2\left(\frac{\sin\theta}{\tilde{r}} - \frac{\partial\theta}{\partial\tilde{s}}\right). \tag{B3}$$

The perturbations Δr and $\Delta\theta$ must be kept small so that the linear expansion of ϵ remains valid. To do this, viscous dissipation is added to the shear elasticity; then, a time step is chosen to create a quasi-elastic response with magnitude proportional to the deviation from equilibrium. Thus, the viscous resistance to membrane deformation regulates the relaxation to the equilibrium shape. Even when the starting shape is far from true equilibrium, the transient force creates a quasi-equilibrium geometry. The relaxation process occurs over discrete time steps Δt; the step size is chosen to ensure that Δr and $\Delta\theta$ are small. The quasi-elastic tension component is introduced into Eq. B3 with the definition,

$$\lambda_m \frac{\partial \tilde{\tau}_s}{\partial \lambda_m} = \tilde{\mu}(\lambda_m^2 + \lambda_m^{-2} + 2t_v/\Delta t), \tag{B4}$$

where t_v is the characteristic viscoelastic time constant. For a true dynamic response of the membrane, t_v would be the viscoelastic response time measured for the red blood cell (18). For computational purposes, t_v is chosen arbitrarily so that $\Delta t/t_v$ at each step is small enough to ensure convergence. This is verified by diminishing the interval until the solution does not change.

The membrane is divided into n segments; at each segment ($i = 1$–n), the changes in r and θ must satisfy:

$$\epsilon + \Delta\epsilon \simeq 0, \tag{B5}$$

where θ and r are related by the geometrical relation,

$$\frac{\partial \tilde{r}}{\partial \tilde{s}} = \cos\theta. \tag{B6}$$

Thus the perturbations in θ and r are governed by

$$\Delta\left(\frac{d\tilde{r}}{d\tilde{s}_0}\right) = -\lambda_m\left[\frac{\cos\theta}{\tilde{r}}\cdot\Delta\tilde{r} + \sin\theta\cdot\Delta\theta\right]. \tag{B7}$$

Finite differences are used to approximate $\Delta(d\tilde{r}/d\tilde{s}_0)$ and $\Delta(d\theta/d\tilde{s}_0)$ through

$$\Delta\left(\frac{d\tilde{r}}{d\tilde{s}_0}\right)_i \equiv (\Delta\tilde{r}_{i+1} - \Delta\tilde{r}_i)/(\tilde{s}_{0_{i+1}} - \tilde{s}_{0_i}) \tag{B8a}$$

$$\Delta\left(\frac{d\theta}{d\tilde{s}_0}\right)_i \equiv (\Delta\theta_{i+1} - \Delta\theta_i)/(\tilde{s}_{0_{i+1}} - \tilde{s}_{0_i}). \tag{B8b}$$

With the finite-difference approximations, a linear system of equations results which consists of $2n$ unknowns (Δr_i, $\Delta\theta_i$) and $2n - 2$ equations. The solution must satisfy two boundary conditions. First, the contact diameter is held fixed; therefore (labeling the membrane in contact with the test surface as $i = 1$),

$$\Delta\tilde{r}_1 = 0. \tag{B9}$$

The second condition is that at some small curvilinear distance δ after the final point $i = n$, the membrane is tangent to the pipette wall where $r = 1$ and $\theta = \pi/2$. The small distance δ is given by

$$\delta = (1 - \tilde{r}_n)\Big/\left(\frac{d\tilde{r}}{d\tilde{s}}\right) = \left(\frac{\pi}{2} - \theta_n\right)\Big/\left(\frac{d\theta}{d\tilde{s}}\right), \tag{B10a}$$

where

$$\frac{d\tilde{r}}{d\tilde{s}} = \cos\theta_n \tag{B10b}$$

$$\frac{d\theta}{d\tilde{s}} = (4\tilde{\tau}_s\sin^2\theta_n + (\tilde{r}_n^2\tilde{P}_c - 1)\cdot\sin\theta_n/\tilde{r}_n)/(\tilde{r}_n^2\tilde{P}_c + 1). \tag{B10c}$$

Thus, the requirement is that the increment in s calculated with either of the difference relations, Δr or $\Delta\theta$, must be compatible. This is formulated as a single equation:

$$\beta + \Delta\beta = 0, \tag{B11}$$

where

$$\beta = (1 - \tilde{r}_n)\frac{d\theta}{d\tilde{s}} - \left(\frac{\pi}{2} - \theta_n\right)\frac{d\tilde{r}}{d\tilde{s}} \tag{B12}$$

$$\Delta\beta = \Delta\tilde{r}\cdot\frac{\partial\beta}{\partial\tilde{r}} + \Delta\theta\cdot\frac{\partial\beta}{\partial\theta} + \Delta\tilde{P}_c\cdot\frac{\partial\beta}{\partial\tilde{P}_c}. \tag{B13}$$

When the increment in s between the instantaneous point n and the tangent contact with the pipette wall becomes large, a new point is added ($n = n + 1$). Each step in the relaxation process consists of solving the system of $2n$ equations for the perturbations in r and θ for the unsupported portion of membrane; then, a trial volume for the capsule cell is calculated. Finally, the pressure is adjusted with the shape calculation repeated until the desired volume is obtained. The whole procedure is followed for a sequence of time steps until the perturbations in r and θ are negligible and the equilibrium shape is found.

This work was supported by the U.S. National Institutes of Health grant HL45099.

Received for publication 13 February 1990 and in final form 15 October 1990.

REFERENCES

1. Evans, E., and V. A. Parsegian. 1983. Energetics of membrane deformation and adhesion in cell and vesicle aggregation. *Annu. NY Acad. Sci.* 416:13–33.
2. Rand, R. P. 1981. Interacting phospholipid bilayers: measured forces and induced structural changes. *Annu. Rev. Biophys. Bioeng.* 10:277–314.

2*a*. Parsegian, V. A. 1974. Long range physical forces in the biological milieu. *Annu. Rev. Biophys. Bioeng.* 2:222–255.

3. Israelachvili, J. N. 1985. Intermolecular and surface forces. Academic Press, San Diego, CA. 296 pp.
4. Evans, E. A. 1985. Detailed mechanics of membrane–membrane adhesion and separation. I. Continuum of molecular cross-bridges. *Biophys. J.* 48:175–183.

4a. Evans, E. A. 1985. Detailed mechanics of membrane–membrane adhesion and separation. II. Discrete kinetically trapped molecular cross-bridges. *Biophys. J.* 48:185–192.

5. Dembo, M., D. C. Torney, K. Saxman, and D. Hammer. 1988. The reaction-limited kinetics of membrane-to-surface adhesion and detachment. *Proc. R Soc. Lond. B* 234:55–83.

6. Irwin, G. R. 1958. Handbuch der Physik, VI. Springer, Berlin. 551–590.

7. Skalak, R., P. R. Zarda, K.-M. Jan, and S. Chien. 1977. Theory of Rouleau formation. *In* Cardiovascular and Pulmonary Dynamics. M. Y. Jaffrin, editor. Institut National de la Santé et de la Recherche Medical (INSERM). 77:299–308.

7a. Skalak, R., P. R. Zarda, K.-M. Jan, and S. Chien. 1981. Mechanics of rouleau formation. *Biophys. J.* 35:771–781.

8. George, J. N., R. I. Weed, and C. F. Reed. 1971. Adhesion of human erythrocytes to glass: the nature of the interaction and the effect of serum and plasma. *J. Cell Physiol.* 77:51–60.

9. Mohandas, N., R. M. Hochmuth, and E. E. Spaeth. 1974. Adhesion of red cells to foreign surfaces in the presence of flow. *J. Biomed. Mater. Res.* 8:119–136.

10. Chien, S., L. A. Sung, S. Kim, A. Burke, and S. Usami. 1977. Determination of aggregation force in rouleaux by fluid mechanical technique. *Microvasc. Res.* 13:327–333.

11. Easty, G. C., D. M. Easty, and E. J. Ambrose. 1960. Studies of cellular adhesiveness. *Exp. Cell Res.* 19:539.

12. McClay, D. R., G. M. Wessel, and R. B. Marchase. 1981. Intercellular recognition: quantitation of initial binding events. *Proc. Natl. Acad. Sci. USA.* 78:4975.

13. Evans, E. A. 1980. Minimum energy analysis of membrane deformation applied to pipette aspiration and surface adhesion of red blood cells. *Biophys. J.* 30:265–284.

14. Evans, E., and A. Leung. 1984. Adhesivity and rigidity of erythrocyte membrane in relation to wheat germ agglutinin binding. *J. Cell Biol.* 98:1201–1208.

15. Sung, K.-L. P., L. A. Sung, M. Crimmins, S. J. Burakoff, and S. Chien. 1986. Determination of junction avidity of cytolytic T cell and target cell. *Science (Wash. DC.).* 234:1405–1408.

15a. Tozeren, A., K.-L. P. Sung, and S. Chien. 1989. Theoretical and experimental studies on cross-bridge migration during cell disaggregation. *Biophys. J.* 55:479–487.

16. Evans, E. A., and K. Buxbaum. 1981. Affinity of red blood cell membrane for particle surfaces measured by the extent of particle encapsulation. *Biophys. J.* 34:1–12.

17. Chien, S., L. A. Sung, S. Simchon, M. M. L. Lee, K.-M. Jan, and R. Skalak. 1983. Energy balance in red cell interactions. *Annu. NY Acad. Sci.* 416:190–204.

18. Evans, E. A., and R. Skalak. 1980. Mechanics and Thermodynamics of Biomembranes. CRC Press, Inc., Boca Raton, FL. 254 pp.

19. Evans, E., D. Berk, A. Leung, and N. Mohandas. 1990. Detachment of agglutinin-bonded red blood cells. II. Measurement of mechanical energies to separate large contact areas. *Biophys. J.* 59:849–860.

20. Evans, E. 1990. Adhesion of surfactant-membrane covered droplets: special features and curvature elasticity effect. *Colloids Surf.* 43:327–347.

21. Waugh, R., and E. Evans. 1979. Thermoelasticity of red blood cell membrane. *Biophys. J.* 26:115–131.

22. Landau, L. D., and E. M. Lifshitz. 1959. Fluid Mechanics. Pergamon Press, London. 536 pp.